ACS OMEGA

http://pubs.acs.org/journal/acsodf

Article

Exploring the Size Effect of Graphene Oxide on Crystallization Kinetics and Barrier Properties of Poly(lactic acid)

Weijiao Jiang, Dandan Chen, Zhihui Xie,* Yue Zhang, Bo Hu, Jian Kang,* Ya Cao, and Ming Xiang

Cite This: *ACS Omega* 2022, 7, 37315−37327

Read Online

ACCESS | Metrics & More | Article Recommendations | Supporting Information

ABSTRACT: Two different sizes of graphene oxide/poly(lactic acid) composites were prepared by the solution flocculation method, and the effect of the size effect of graphene oxide on the crystallization, barrier, and mechanical properties of poly(lactic acid) was investigated by various characterization methods. The results of the crystallization behavior test show that the size change of graphene oxide has little effect on the nucleation effect of poly(lactic acid). Increasing the size of graphene oxide can promote the crystal growth, so as to improve the crystallization ability of poly(lactic acid). The test results of mechanical properties and barrier properties show that increasing the size of graphene oxide can provide a larger interfacial surface area and transmit stress more effectively, which can greatly improve the modulus of poly(lactic acid). At the same time, because of this, the diffusion path of gas molecules in poly(lactic acid) can be longer and more tortuous, so as to improve the barrier performance of poly(lactic acid).

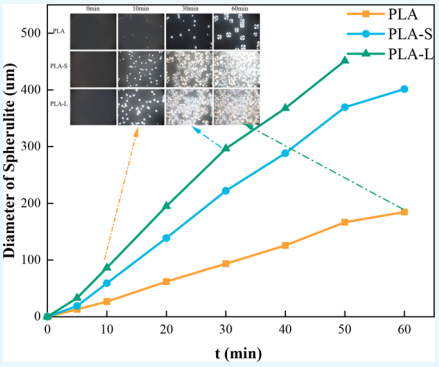

1. INTRODUCTION

Polymer materials are widely used in people's daily life. The polymer materials used more often are mainly petroleum-based resins. Most of the monomers of these petroleum-based resins are derived from petroleum. The large-scale use of petroleum-based resins brings a lot of waste, and petroleum is a nonrenewable resource, which also leads to the waste of petroleum resources. Most polymer materials are nondegradable polymer materials. Because of their nondegradability, their mass waste will inevitably lead to white pollution and bring greater pressure on the environment.[1] Poly(lactic acid) (PLA), a biodegradable and renewable biopolymer, undoubtedly provides a good solution to this environmental and energy problem.

The monomer of PLA is lactic acid, which is mainly derived from plants. It has a wide range of sources and is renewable. Therefore, PLA is an excellent potential substitute for petroleum-based resins.[2] The main chain of PLA contains a large number of ester groups and methyl side groups, so the molecular chain is rigid and the mobility of the molecular chain is weak, which makes the glass transition temperature (T_g) of PLA larger so that the PLA has poor heat resistance, poor crystallization ability, and poor toughness.[3−6] The barrier properties of PLA also fail to meet the commercial requirements. These shortcomings seriously limit the wide application of PLA. At present, PLA is mainly used in the medical industry. To broaden its application, our predecessors have done much research to improve the performance of PLA, mainly through chemical modification, modification with other polymers, adding nanofillers,[2,7,8] etc. Adding nanofillers for modification is a relatively simple and efficient method. Adding a small amount can achieve the goal of greatly improving performance and does not affect the key properties of PLA.[9]

Graphene oxide (GO) is a two-dimensional sheet of carbon material and a derivative of graphene. It has a honeycomb structure and is mainly composed of sp^2 and sp^3 hybrid carbon atoms. As a result of its high density of the surface electron cloud, GO is impermeable, which makes allows it to have an excellent barrier performance. The surfaces of GO flakes contain a large number of epoxy groups, hydroxyl groups, and of carboxyl groups at the edges,[10−12] which allows the flakes to have more active sites, be better dispersed in the matrix or solution, and have stronger interfacial binding ability compared to graphene.[13] Meanwhile, GO has a high modulus (mean value of 32 GPa) and fracture strength (mean value of 80 MPa) and has a great potential for reinforcing polymers.[14]

Huang et al. prepared randomly dispersed GO/PLA composites and found that when the GO content was 1.37 vol %, the permeability coefficients of O_2 and CO_2 decreased by 45% and 68%, respectively, which substantially improved the barrier properties of PLA.[15] Geng et al. investigated the effect of GO content on the crystallization behavior of GO/PLA composites and found that GO can act as a nucleating agent for PLA. With the increase of GO content, the

Received: June 20, 2022
Accepted: October 4, 2022
Published: October 12, 2022

https://doi.org/10.1021/acsomega.2c03830
ACS Omega 2022, 7, 37315−37327

Scheme 1. Schematic Diagram of DSC Program Setting for the Cooling and Isothermal Process

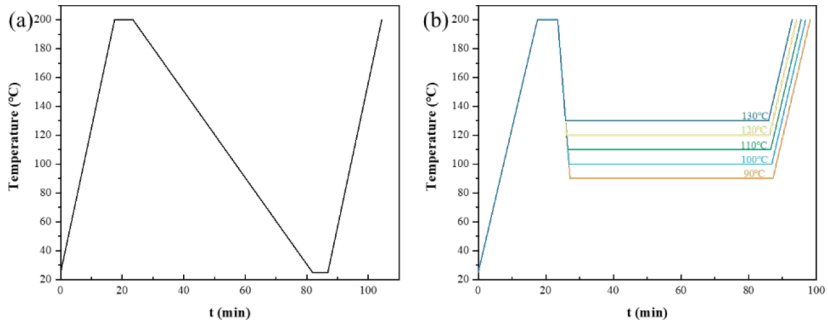

crystallinity of PLA increased from 4.34% to 49.01%. Obviously, GO can significantly improve the crystallinity of PLA.[16] Zheng et al. studied the effect of amidated GO on the properties of PLA and found that the addition of 0.3 wt % could increase the crystallinity of PLA by 34.1% and the elongation at break and impact strength by 47.32 and 41.27%.[17] A comparison table of the barrier performance enhancement of PLA by GO and other fillers (see Supporting Information) shows that GO has a greater advantage in enhancing the barrier performance of PLA. Obviously, GO is an excellent modified filler for PLA.

Previous studies mainly focused on the differences in the effects of the content of GO and preparation methods of GO on the properties of PLA, and there were few studies on the effects of size variation of GO on the properties of PLA. In this paper, the effect of GO size change on the crystallization kinetics of PLA was systematically studied by differential scanning calorimetry (DSC), polarizing light microscopy (PLM), and small angle X-ray scattering analysis (SAXS), and the effect of GO size change on the properties of PLA was explored by other characterization methods. The crystallization dynamics study reveals that the size change of GO mainly affects the crystal growth process and then the crystallization behavior of PLA. As a result of the different sizes of GO, the interface area between GO and PLA is different, so there are differences in thermal properties, mechanical properties, and barrier properties.

2. EXPERIMENTAL SECTION

2.1. Materials. The L-poly(lactic acid) with the trade name of 4043D was purchased from the American Nature Work Company. Large-scale graphene oxide (GO-L) and small-scale graphene oxide (GO-S) were purchased from Deyang Alkene Carbon Technology Co., Ltd., China. *N*,*N*-Dimethylformamide (DMF) was ordered from Chengdu Cologne Reagent Co., Ltd., China. The distillation was done in the laboratory.

2.2. Preparation of Samples. To make GO-L and GO-S uniformly dispersed in PLA, GO/PLA composites with an addition of 0.1 wt % were prepared by the solution flocculation method.[15] First, 10 mg of GO was weighed and then dispersed in 200 mL of DMF solution by ultrasound to obtain a well-dispersed GO suspension. At the same time, 10 g of PLA was dissolved in 200 mL of DMF solution at 100 °C with stirring. After the PLA was completely dissolved, the dispersed GO suspension was added to it, and the stirring was continued for 30 min. After cooling to room temperature, the mixed solution was added to distilled water for sedimentation, followed by vacuum filtration, and the filtered sediment was placed in a 50 °C vacuum oven to remove residual solvent. Finally, the dried powder samples were pressed into cast pieces by compression molding at 200 °C. In the following text, the pure PLA sample is denoted as PLA, and the composite material added with GO-L is denoted as PLA-L. Likewise, the composite material added with GO-S is denoted as PLA-S.

2.3. Characterization. To compare the dispersions of graphene oxide with different sizes in PLA, the samples were quenched in liquid nitrogen, and their sections were sprayed with gold. Field emission scanning electron microscopy (SEM) (FEI Inspect F microsope) was used to observe the surface morphology of the samples.

X-ray photoelectron spectroscopy (XPS) (Thermo Scientific K-Alpha 2.4 spectrometer) was used to measure the contents of C and O elements to further measure the degree of oxidation.

Thermogravimetric (TG) analysis (METTLER TOLEDO-TGA2 analyzer) was used to measure the thermal stability of graphene oxide. The test procedure was to weigh 3−8 mg of the sample, and in a nitrogen atmosphere, the sample was heated from 35 to 800 °C with a heating rate of 10 °C/min.

The test was carried out using X-ray diffraction (XRD) (Ultima IV diffractometer produced by Rigaku Corporation of Japan). Cu Kα X-ray was used as the radiation source. The wavelength was 0.15416 nm. The test range was 5−30°, and the sample scanning speed was 10°/min. The interlamellar spacing (d) of graphene oxide can be calculated from the Bragg equation:[18]

$$d = \frac{n\lambda}{2 \sin \theta} \quad (1)$$

where λ is the wavelength of the X-ray, θ is the angle between the incident X-ray and the corresponding crystal plane, and n is the diffraction order.

Ultraviolet−visible (UV) spectroscopy (Shimadzu UV-1800 spectrophotometer, Shimadzu Co., Japan) was used to compare the dispersibilities of GO of different sizes in DMF solution. The GO was dispersed in DMF solution by ultrasonication for 2 h, and then the concentration was adjusted to 0.025 mg/mL. The test range was 280−1000 nm, and the scan speed was medium. The sampling interval is 0.5 nm. To compare the stability of GO of different sizes in DMF solution, the uniformly dispersed suspension left to stand for one month, and the sedimentation was observed.

The effect of the size change of GO on the rheological behavior of PLA was investigated using a modular intelligent advanced rotational rheometer MCR302 produced by Anton Paar Co., Ltd., in Austria. The samples were pressed into small discs with a diameter of 25 mm and a thickness of 1 mm and were vacuum-dried at 60 °C for 6 h. In order to ensure that the

https://doi.org/10.1021/acsomega.2c03830
ACS Omega 2022, 7, 37315−37327

rheological test was in the linear rheological region, the experimental conditions were set as follows: first, the test program was set to the frequency sweep of the melt, and then the temperature was set to 190 °C. The fixed strain was 1%, and the sweep frequency range was 0.1−600 rad/s.

Differential scanning calorimetry (DSC) (DSC 3+/500, METTLER TOLEDO, Switzerland) was used to study the effect of the size change of graphene oxide on the crystallization behavior of PLA.

2.3.1. Routine DSC Test. A total of 3−5 mg of sample was placed into the crucible. The test procedure is to raise the temperature from 25 to 200 °C at the heating rate of 10 °C/min, then hold isothermally at 200 °C for 5 min, then lower the temperature to 25 °C at the cooling rate of 3 °C/min, remain at 25 °C for 5 min, and finally raise the temperature to 200 °C at the heating rate of 10 °C/min. The corresponding DSC program setup schematic is shown in Scheme 1a.

2.3.2. Isothermal Crystallization Test. The samples were first raised from room temperature to 200 °C at a rate of 10 °C/min and held for 5 min to eliminate thermal history. Then, the temperature was rapidly lowered to the specified isothermal crystallization temperature (90 °C, 100 °C, 110 °C, 120 °C, 130 °C) at a speed of 30 °C/min and kept at that temperature for 1 h to ensure the completion of the crystallization process. Finally, it was raised to 200 °C at a rate of 10 °C/min. The corresponding DSC program setup schematic is shown in Scheme 1b.

The crystallinity (X_c) of the sample can be calculated by the formula:

$$X_c = \frac{\Delta H_m - \Delta H_{cc}}{\Delta H_f^0} \tag{2}$$

ΔH_m is the melting enthalpy of the sample, and ΔH_{cc} is the cold crystallization enthalpy of the sample. ΔH_f^0 is the melting enthalpy of 100% complete crystallization of the PLA sample, which is 93.6 J/g.[19]

The relative crystallinity (X_t) represents the crystallization process at different times, and its calculation formula is as follows:

$$X_t = \frac{\int_0^t (\mathrm{d}H/\mathrm{d}t)\mathrm{d}t}{\int_0^\infty (\mathrm{d}H/\mathrm{d}t)\mathrm{d}t} \tag{3}$$

dH is the corresponding enthalpy value when the crystallization time is dt, t represents the time consumed in the crystallization process, and ∞ represents the time to complete the crystallization.[20]

The Avrami equation is used to describe the crystallization process, and its logarithmic variation is as follows:[21,22]

$$\ln[-\ln(1 - X_t)] = \ln k + n \ln t \tag{4}$$

where X_t is the relative crystallinity, n is the Avrami index, and k is the crystallization rate parameter.

The half-crystallization time ($t_{1/2}$) is the time consumed for the relative crystallinity to reach 50%. Generally speaking, the shorter the half-crystallization time, the faster the crystallization rate. The half-crystallization time can be obtained by the following formula:[23]

$$t_{1/2} = \left(\frac{\ln 2}{k}\right)^{1/n} \tag{5}$$

The crystallization rate ($G_{1/2}$) is obtained by calculating the reciprocal of $t_{1/2}$, and the calculation formula is as follows:

$$G_{1/2} = \frac{1}{t_{1/2}} \tag{6}$$

To visually compare the effect of the size of graphene oxide on the crystallization process of PLA, the isothermal crystallization process of the samples was observed using a polarizing microscope (PLM) with a hot stage (Nikon Eclipse LV100N, Japan). First, it was raised from room temperature to 200 °C and held for 5 min to eliminate the thermal history, and then it was rapidly cooled down to 140 °C at a rate of 50 °C/min and held isothermally for 1 h. Photos were taken immediately when the sample reached 140 °C and then every 10 min.

The long period (L_p) of the samples was measured using a two-dimensional small-angle X-ray scattering instrument (2D-SAXS, Xenocs, France). The X-ray source was a Cu Kα target (λ = 0.154 nm), and the distance between the sample and the detector was 2500 mm. The sample was placed perpendicular to the emission direction of the light source, and the exposure time was 10 min. The average long period (L_p) can be obtained by the Bragg equation:[24,25]

$$L_p = \frac{2\pi}{q_{\max}} \tag{7}$$

where $q_{\max}$ is the scattering vector corresponding to the maximum scattering intensity on the 1D-SAXS curve.

The lamellar thickness (L_c) of the crystal region can be calculated from the following formula:[26]

$$L_c = L_p X_c \tag{8}$$

The specimens were pressed into rectangular splines of 50 mm × 10 mm × 1 mm and tested on a universal material testing machine (CMT6104, MTS SYSTEMS (China) Co., Ltd., U.S.A.) at room temperature. The stretching rate was 10 mm/min, and the gauge length was 10 mm.

The gas barrier performance of the sample was measured by the differential pressure gas permeability meter VAC-V1 produced by Jinan Languang Electromechanical Technology Co., Ltd. The samples were cut into square splines of 40 mm × 40 mm × 1 mm, tand he test temperature was 23 °C. The test atmosphere was O_2, and the degassing time of the high-pressure and low-pressure chambers was 8 h.

3. RESULTS AND DISCUSSIONS

3.1. Characterization of Different Sizes of Graphene Oxide. The size distributions of two different sizes of graphene oxide were measured by a TEM test, and the corresponding results are shown in Figure 1. The distribution shows that the size of GO-L is mainly distributed between 500 and 1500 μm and the size of GO-S is mainly distributed between 100 and 700 μm. Apparently the size of GO-L is larger than that of GO-S.

Figure 2a,b is the thermogravimetric curves of two different sizes of GO. It can be seen from Figure 2b that the degradation of GO can be divided into three stages. When the temperature is lower than 100 °C, the mass loss of GO is mainly caused by the volatilization of water molecules adsorbed on its surface. When the temperature reaches 150 to 250 °C, the oxygen-containing functional groups on the surface of GO are degraded.[27] When the temperature is higher than 250 °C

https://doi.org/10.1021/acsomega.2c03830
ACS Omega 2022, 7, 37315−37327

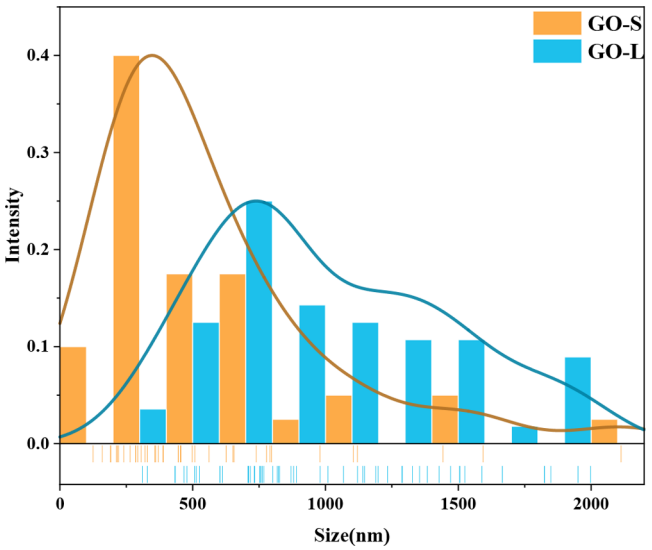

Figure 1. Size distributions of GO nanosheets.

and lower than 300 °C, the mass loss of GO is mainly caused by the decomposition of more stable oxygen-containing functional groups and the destruction of a small amount of defective carbon structures on the main chain. It can be seen from Figure 2a that the carbon residue of GO-S is 46.51% and that of GO-L is 42.74%. Compared with GO-S, GO-L is more degraded in the process of heating, and the thermal stability of GO-S is slightly better than that of GO-L. This indicates that the oxidation degree of GO-L is higher than that of GO-S.

Table 1. Element Content of GO Nanosheets Obtained from the XPS Energy Spectrum

sample	name	peak BE (eV)	atomic (%)	A_c/A_0
GO-S	C 1s	286.09	71.06	2.46
	O 1s	532.90	28.94	
GO-L	C 1s	285.92	70.68	2.41
	O 1s	532.75	29.32	

To quantitatively compare the oxidation degrees of GO-S and GO-L, XPS spectroscopy was performed on GO-S and GO-L. The XPS spectra of GO-S and GO-L are shown in Figure 2c, and the corresponding calculation results of the element contents are shown in Table 1. Only the signal responses of C and O elements can be observed in the XPS spectrum. In addition, it can be seen from Table 1 that the C/O ratio of GO-S is 2.46, and the C/O ratio of GO-L is 2.41. It can be concluded that the C/O of GO-L is smaller than that of GO-S, which can prove that the oxidation degree of GO-L is slightly larger than that of GO-S.

It can be seen from Figure 2d that both GO-S and GO-L have a strong diffraction peak of the (001) crystal plane of GO. From this characteristic peak, the interlamellar spacing of GO can be calculated. The lamellar spacing of GO-S is 0.95 nm, and the lamellar spacing of GO-L is 0.94 nm. The lamellar spacing of GO-S is larger than that of GO-L, which is related to the slightly higher oxidation degree of GO-L than GO-S.

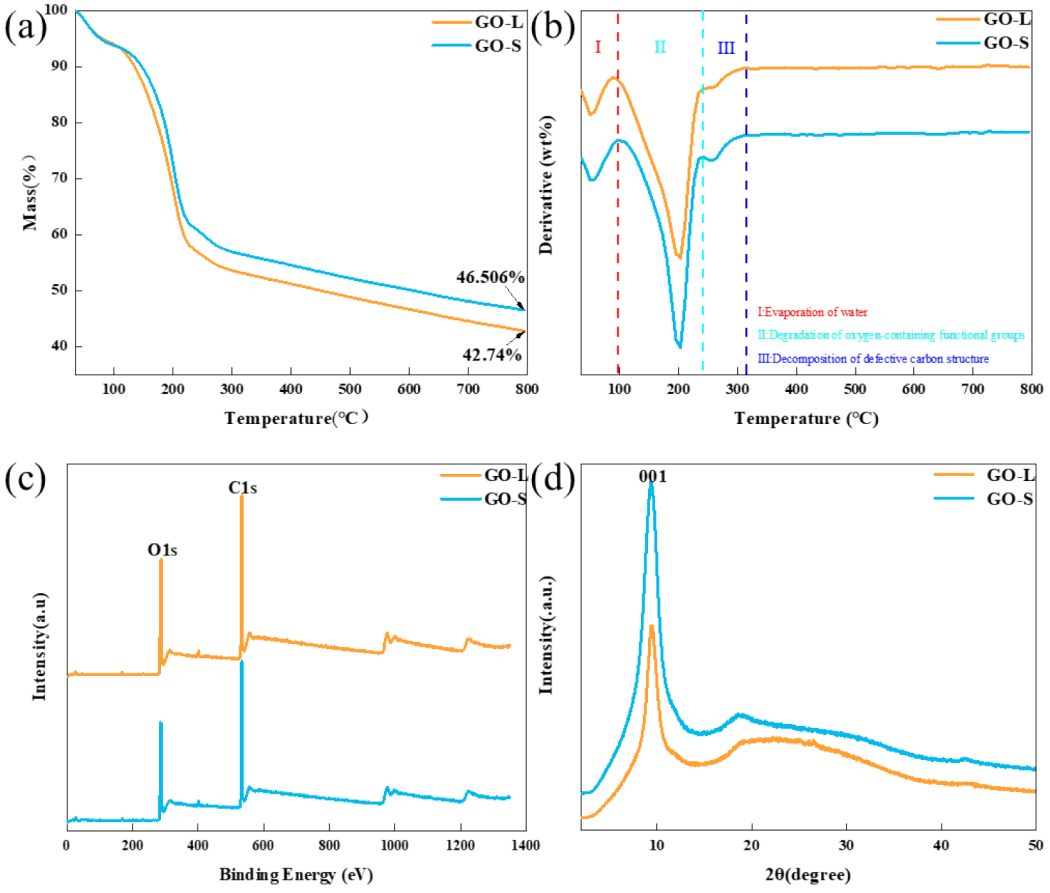

Figure 2. (a) Thermogravimetric curves of GO, (b) corresponding derivative thermogravimetric curves, (c) XPS energy spectrum of GO nanosheets, and (d) XRD patterns of GO nanosheets.

https://doi.org/10.1021/acsomega.2c03830
ACS Omega 2022, 7, 37315−37327

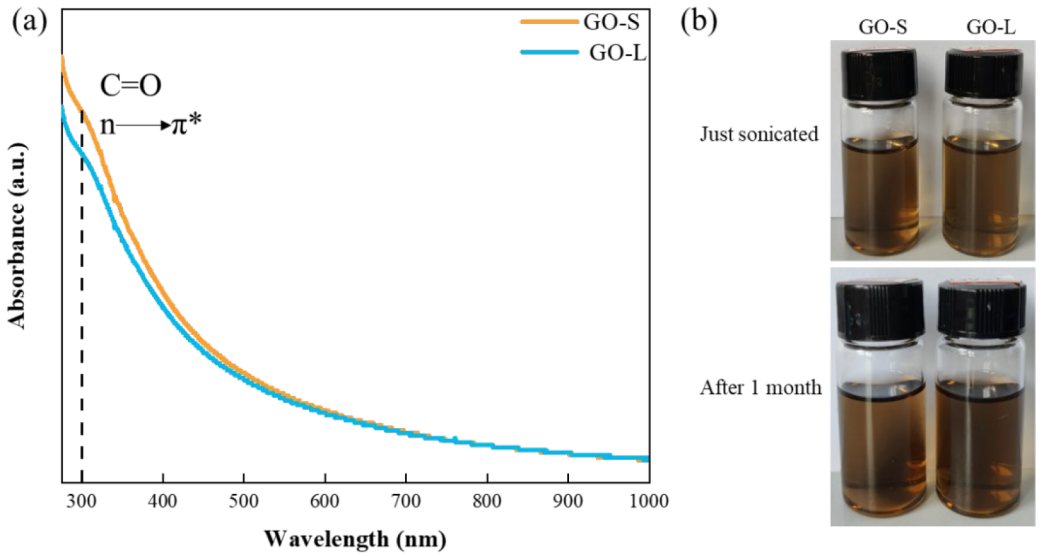

Figure 3. (a) UV−vis absorption spectra of graphene oxide dispersed in DMF by means of bath ultrasonication (2 h) and (b) digital pictures of graphene oxide dispersed in DMF through bath ultrasonication (2 h). Top: dispersions immediately after sonication. Bottom: dispersions 1 month after sonication.

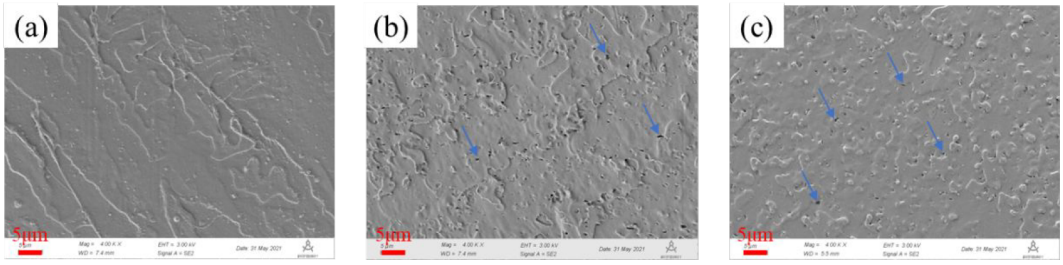

Figure 4. SEM images of the (a) neat PLA, (b) PLA-S, and (c) PLA-L.

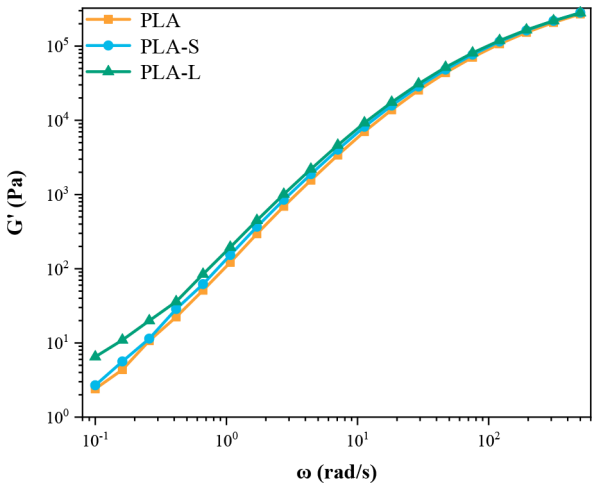

Figure 5. Variation of storage modulus (G') as a function of frequency for neat PLA and its nanocomposites.

Because the GO/PLA composites were prepared by the solution method, in order to ensure that GO can be uniformly dispersed in PLA, the dispersibility and stability of GO-S and GO-L in the DMF solution were first explored. The dispersion of GO with different sizes in DMF solution was studied by UV−vis absorption spectrsocopy. The test results are shown in Figure 3. The UV−vis spectra of GO show two characteristic absorption peaks, which can be used as a recognition means. The shoulder peak at 231 nm corresponds to the $\pi \rightarrow \pi^*$ transition of the aromatic C−C bond; the shoulder peak at 300 nm corresponds to the n $\rightarrow \pi^*$ transition of the C═O bond.[28] However, because of the strong absorption of DMF in the range of 200−265 nm, the instrument cannot perform proper compensation. The lower limit of the measurement of the ultraviolet wavelength tested here is 280 nm. As can be seen from Figure 3a, the absorbance of GO-S at 300 nm is slightly greater than that of GO-L, mainly because the reduction of the size of GO will enhance the UV absorption of GO. This can be understood as the color enhancement effect caused by size reduction.[29] In general, GO-S and GO-L can be well dispersed in the DMF solution. It can be seen from Figure 3b that no obvious sedimentation of the GO suspension was observed after being placed under ultrasonic treatment for one month. It can be concluded that both GO-S and GO-L can be uniformly and stably dispersed in the DMF solution.

3.2. Dispersion Characterization. It can be seen from Figure 4 that the fractured surface of the pure PLA sample is relatively smooth, while the fractured surface of the sample after adding GO is relatively rough. Some irregular holes can be seen on the fractured surfaces of PLA-S and PLA-L, which are mainly due to the GO nanosheets being pulled out during the brittle fracture process.[30] The sizes of these holes are basically between 1 and 2 μm, which is close to the size of monolithic GO. It can be seen that both GO-S and GO-L are well dispersed in PLA. The result shows that when the filler

https://doi.org/10.1021/acsomega.2c03830
ACS Omega 2022, 7, 37315−37327

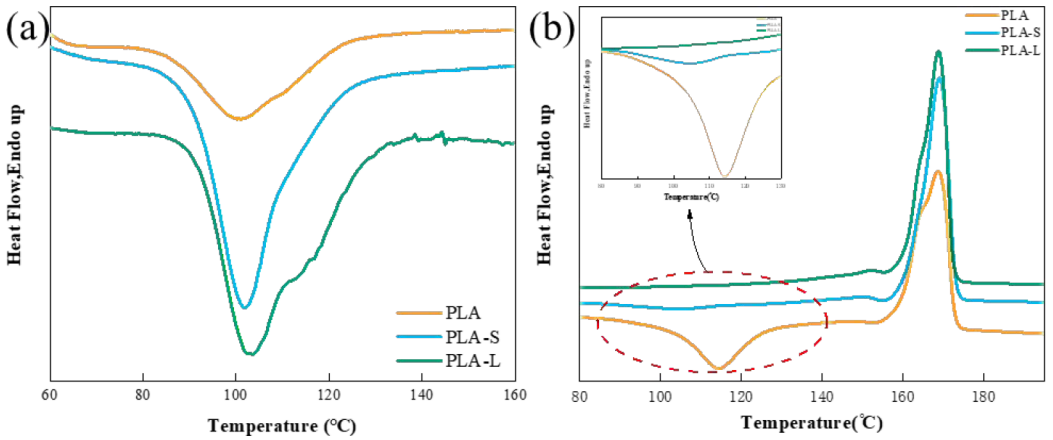

Figure 6. (a) DSC cooling curves and (b) subsequent heating curves of neat PLA and its nanocomposites.

Table 2. Crystallization and Melting Parameters of Neat PLA and Its Nanocomposites

sample	ΔH_m(J/g)	ΔH_c(J/g)	X_c (%)
PLA	37.91	21.86	17.1
PLA-S	42.49	3.12	42.1
PLA-L	45.61		48.7

content was 0.1 wt %, the size change of GO had little effect on its dispersion in PLA.

3.3. Crystallization Kinetics. To verify that both GO-S and GO-L have no inhibitory effect on the crystallization behavior of PLA under the loading of 0.1 wt %, the rheological behaviors of PLA, PLA-S, and PLA-L were measured, and the corresponding result is shown in Figure 5. For the polymer composite system with nanoparticles, when the loading of nanoparticles exceeds a critical value (this critical value is called the rheological percolation threshold), due to the interaction between nanoparticles, nanoparticles will form a network structure in the polymer matrix. The formation of this network structure will greatly inhibit the movement of molecular chains and hinder the crystallization of polymers. The rheological percolation threshold can be determined by the load corresponding to the plateau region where viscous fluid transforms into a solid-like material in the low-frequency region of the rheological curve.[31,32] It can be seen from Figure 5 that, in the low-frequency region, the storage modulus of PLA, PLA-S, and PLA-L increases with the increase of frequency, and 0.1 wt % is below the rheological percolation threshold. This result shows that the addition of GO-S and GO-L will not hinder the crystallization of the polymer when the load is 0.1 wt %.

The conventional DSC curves of PLA, PLA-S, and PLA-L are shown in Figure 6, and the corresponding parameters are shown in Table 2. It can be seen from Figure 6a that, after adding GO-S and GO-L, the peak intensity of the crystallization peak of PLA is significantly improved, which means that the crystallinity of PLA is significantly improved, and the low-temperature crystallization peak (corresponding to the peak intensity of the α'-form) increased more obviously, indicating that the addition of GO-S and GO-L can significantly improve the crystallinity of PLA and the crystallization ability of the α' crystal. From Figure 6b, it can be observed that, compared with PLA, the cold crystallization

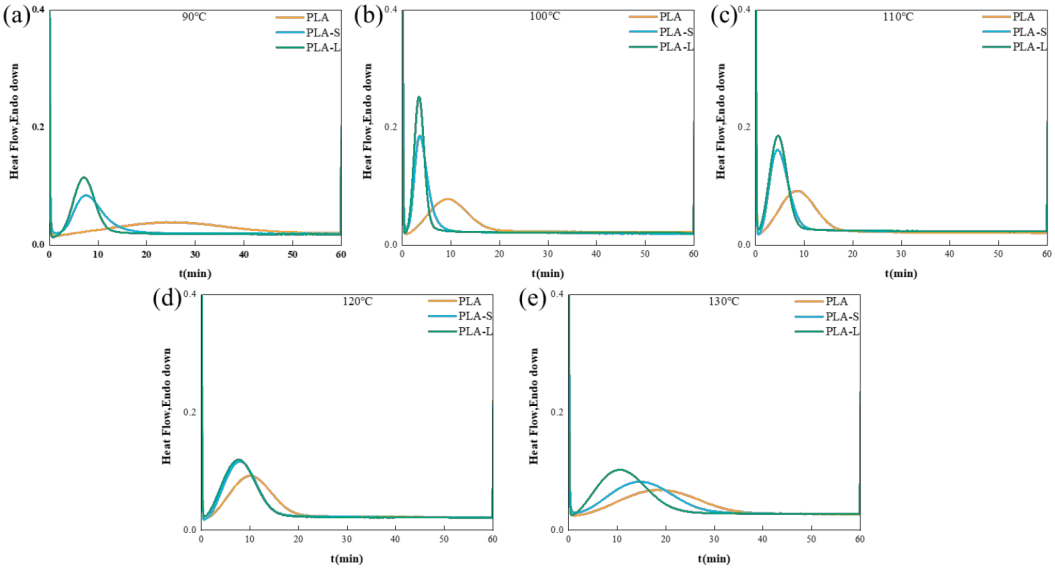

Figure 7. Crystallization curves of neat PLA and its nanocomposites after being isothermally crystallized at (a) 90 °C, (b) 100 °C, (c) 110 °C, (d) 120 °C, and (e) 130 °C for 60 min.

https://doi.org/10.1021/acsomega.2c03830
ACS Omega 2022, 7, 37315−37327

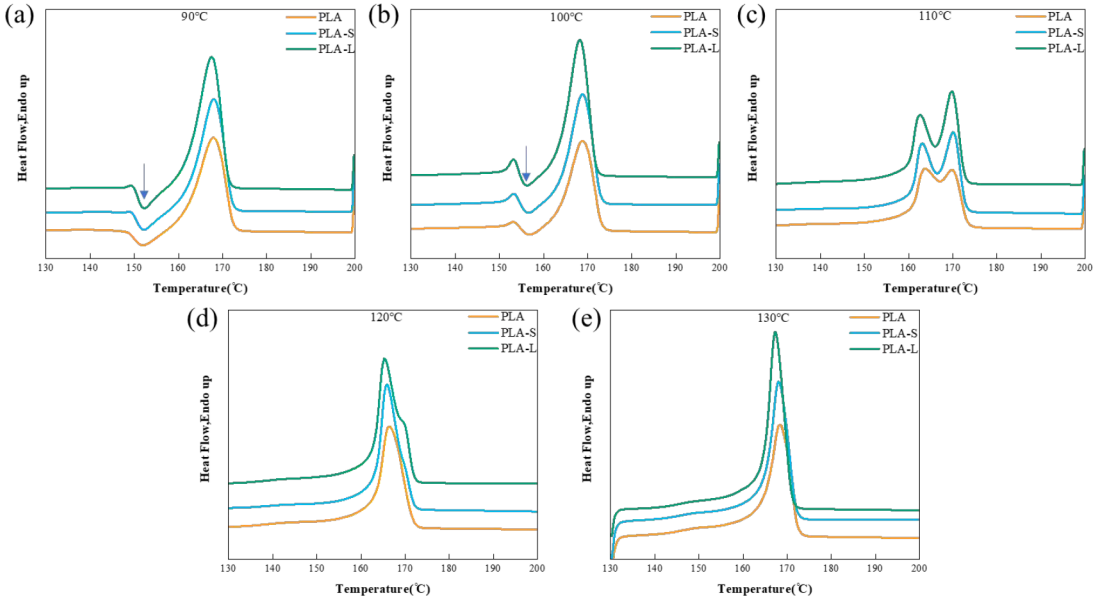

Figure 8. Heating curves of neat PLA and its nanocomposites after being isothermally crystallized at (a) 90 °C, (b) 100 °C, (c) 110 °C, (d) 120 °C, and (e) 130 °C for 60 min.

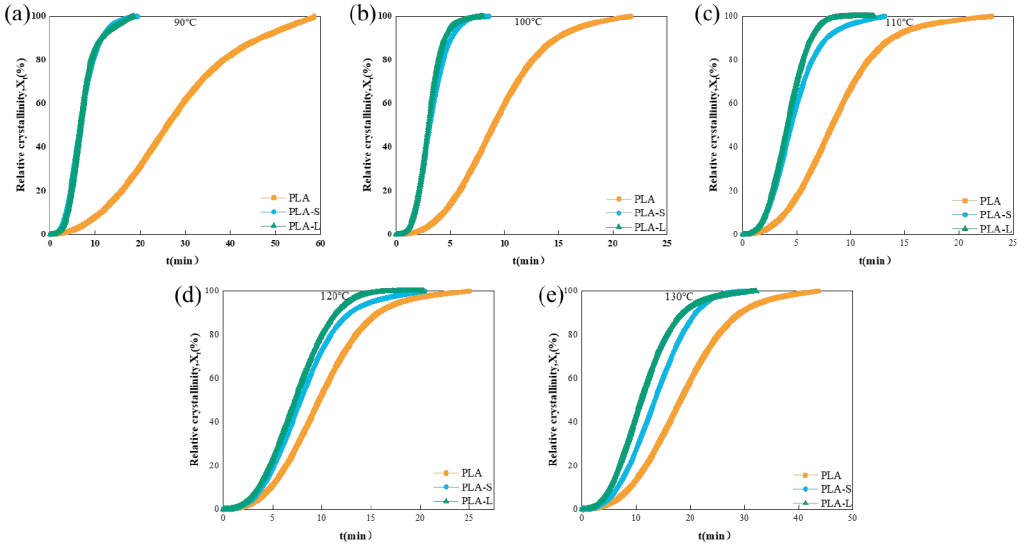

Figure 9. Relative crystallinity as a function of crystallization time of neat PLA and its nanocomposites after being isothermally crystallized at (a) 90 °C, (b) 100 °C, (c) 110 °C, (d) 120 °C, and (e) 130 °C for 60 min.

peak of PLA-S is significantly weakened, and PLA-L has almost no cold crystallization peak. As shown in Table 2, the crystallinity of pure PLA is 17.1%, that of PLA-S is 42.1%, and that of PLA-L is 48.7%. This indicates that GO-L can improve the crystallization ability of PLA more than GO-S.

To further explore the effect of the size change of graphene oxide on the crystallization kinetics of PLA, pure PLA, PLA-S, and PLA-L were subjected to isothermal crystallization treatment at different temperatures, and the corresponding results are shown in Figure 7 and Figure 8. It can be seen from Figure 7 that the peak widths of the isothermal crystallization peaks of PLA-L and PLA-S are smaller than those of PLA, and the peaks are sharper. This indicates that GO can accelerate the crystallization process of PLA. Double-melting behavior is observed from the melting curves of Figure 8a–c, which is mainly the result of melt recrystallization.[33] When the temperature is lower than 120 °C, the crystal form formed by isothermal crystallization of PLA is the α'-form, which is accompanied by the formation of the α crystal during the melting process, and subsequent α crystals melt at higher temperatures. A downward exothermic peak (indicated by the arrow in Figure 8) can be observed on the melting curves of PLA, PLA-S, and PLA-L at 90 and 100 °C after being held isothermally for 60 min, which is mainly because the recrystallization rate of the α'-form into the α-form is higher than the melting rate of the α'-form. Therefore, a small α-form crystallization peak can be observed in the melting region.[34] When the temperature is 120 °C and above, the crystal form formed by isothermal crystallization of PLA is the α-form, and its melting curve has only one single melting peak. However, the melting curves of PLA-S and PLA-L after isothermal crystallization at 120 °C for 60 min still show the phenomenon of the double-melting peak. This may be due to the fact that although the addition of GO-S and GO-L can speed up the

https://doi.org/10.1021/acsomega.2c03830
ACS Omega 2022, 7, 37315−37327

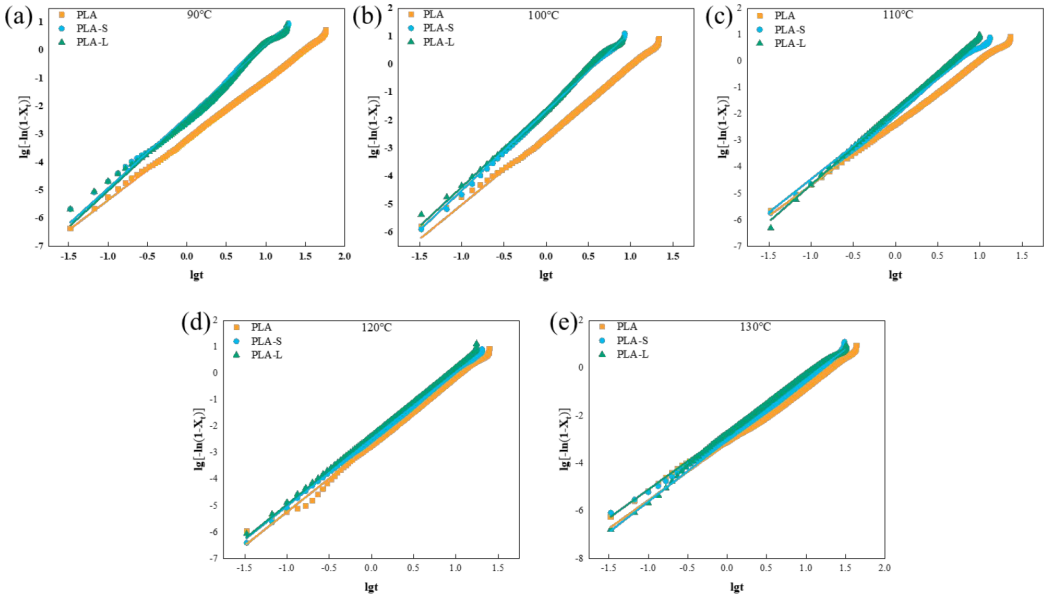

Figure 10. Avrami plots of $\ln[-\ln(1-X_t)]$ versus $\ln t$ of neat PLA and its nanocomposites after being isothermally crystallized at (a) 90 °C, (b) 100 °C, (c) 110 °C, (d) 120 °C, and (e) 130 °C for 60 min.

Table 3. Avrami Parameters for Isothermal Crystallization of Neat PLA and Its Nanocomposites

sample	T_c (°C)	$t_{1/2}$ (min)	$G_{1/2}$ (min)	n	k (min^{-n})	ΔH_m (J/g)	X_c (%)
PLA	90.0	26.1	0.04	2.1	6.30×10^{-4}	36.4	38.9
	100.0	9.0	0.11	2.5	2.87×10^{-3}	37.5	40.1
	110.0	8.3	0.12	2.3	4.50×10^{-3}	39.9	42.6
	120.0	9.7	0.10	2.5	1.98×10^{-3}	45.2	48.3
	130.0	18.2	0.06	2.4	6.89×10^{-4}	52.5	56.0
PLA-S	90.0	6.7	0.15	2.5	4.23×10^{-3}	41.6	44.4
	100.0	3.1	0.32	2.8	2.20×10^{-2}	42.2	45.1
	110.0	4.5	0.22	2.5	1.18×10^{-2}	43.8	46.8
	120.0	7.8	0.13	2.5	3.30×10^{-3}	48.7	52.0
	130.0	13.4	0.07	2.6	9.33×10^{-4}	55.9	59.7
PLA-L	90.0	6.7	0.15	2.6	3.70×10^{-3}	46.9	50.1
	100.0	3.0	0.34	2.8	2.67×10^{-2}	48.2	51.5
	110.0	4.1	0.24	2.8	1.34×10^{-2}	48.4	51.7
	120.0	7.2	0.14	2.6	4.31×10^{-3}	53.1	56.7
	130.0	10.8	0.09	2.4	1.97×10^{-3}	62.1	66.3

crystallization of PLA, the degree of perfection of the crystal structure is relatively reduced. Therefore, during the melting process, imperfect crystals tend to melt to form perfect ones and then melt again.

To compare the influence of GO-S and GO-L on the crystallization rate of PLA, formula (3) was first used to obtain the cumulative curves of X_t and t of PLA, PLA-S, and PLA-L, as shown in Figure 9. Then, the relationship between $\ln[-\ln(1-X_t)]$ and $\ln t$ (see Figure 10) of PLA, PLA-S, and PLA-L is obtained by using the Avrami eq 4. The Avrami index (n) and crystallization rate parameter (k) were obtained by the slope and intercept of the fitting curve. The crystallization rate ($G_{1/2}$) can be calculated by formulas 5and 6. The parameters obtained above are shown in Table 3. It can be seen from Table 3 and Figure 11 that the $t_{1/2}$ of PLA-S and PLA-L is significantly reduced, and the crystallization rate is significantly accelerated. This rule is especially obvious for samples treated at a lower temperature, which may be due to the fact that GO-S and GO-L can promote the growth of PLA crystals. The lower temperature is conducive to the nucleation of the polymer matrix itself, but the crystal growth rate is slower. After adding GO, the crystal growth rate of PLA itself at low temperature is improved and the crystal nucleus density increases, so the crystallization rate of PLA is greatly increased. The higher temperature is conducive to crystal growth and is

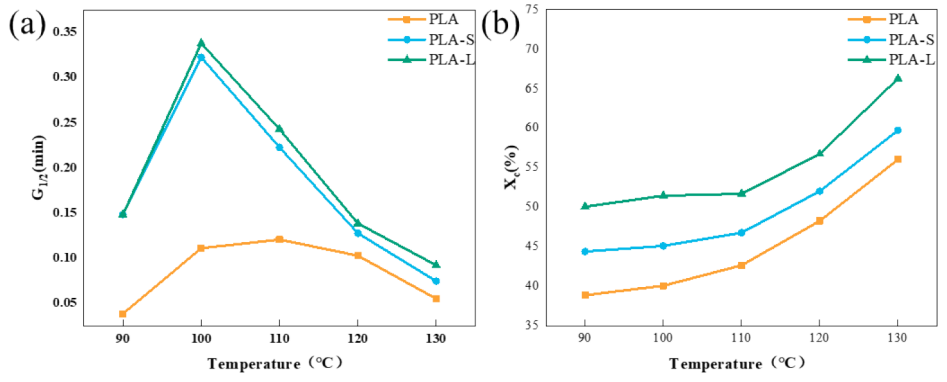

Figure 11. (a) Crystallization rate, $G_{1/2}$, and (b) crystallinity, X_c, of samples.

https://doi.org/10.1021/acsomega.2c03830
ACS Omega 2022, 7, 37315−37327

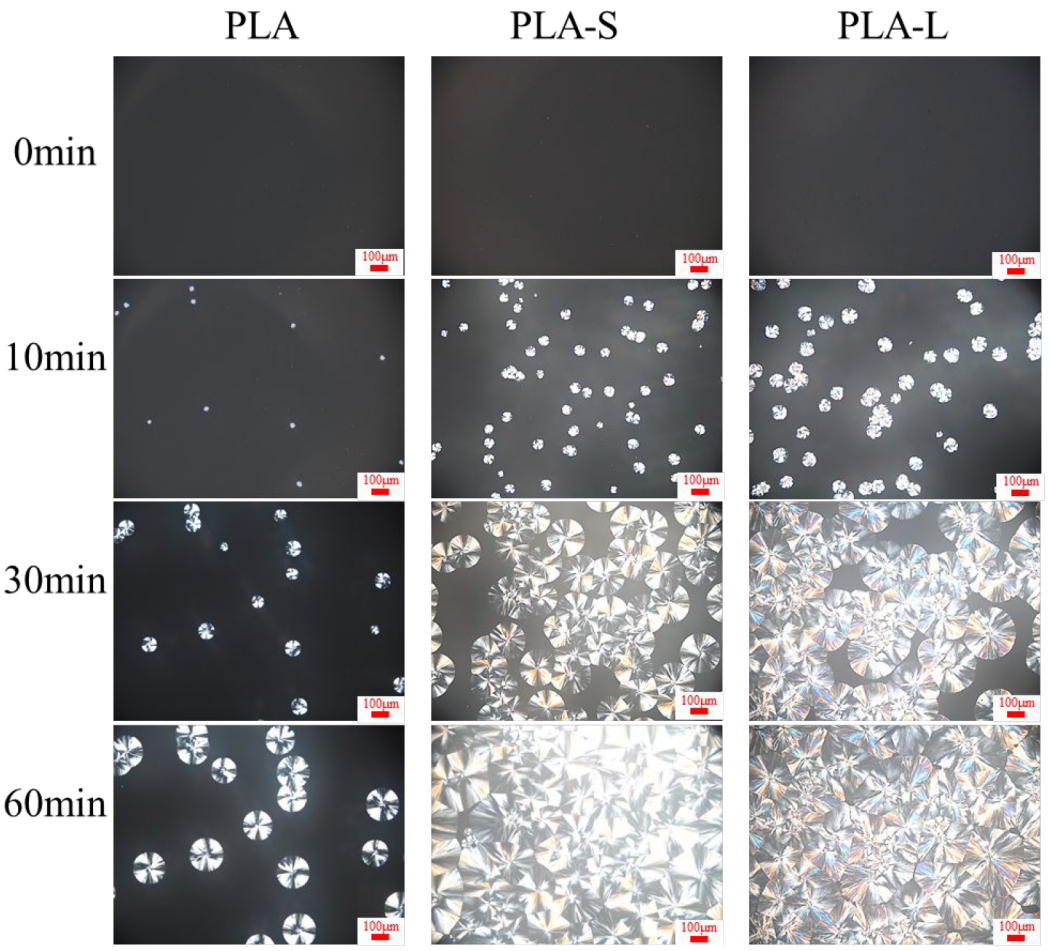

Figure 12. PLM images during the time evolution of isothermal crystallization of all samples at 140 °C.

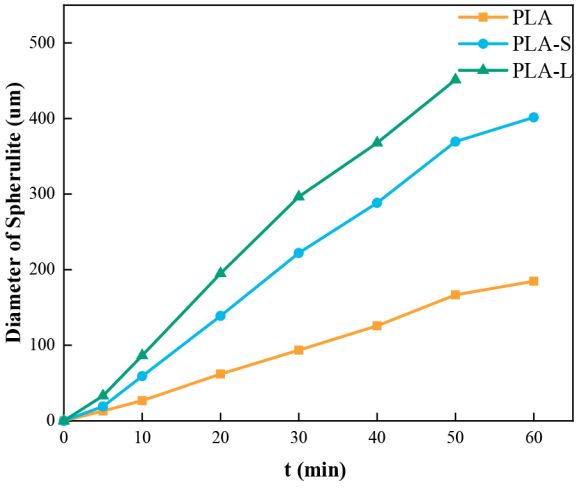

Figure 13. Relationship between spherulite diameter and time of all samples after isothermal crystallization at 140 °C.

not conducive to crystal nucleation. Relatively speaking, the promotion of GO to the crystal growth of PLA is weakened, and the improvement of GO to the crystallization speed of PLA is reduced. It can also be seen from Figure 11 that the crystallization rate and crystallinity of PLA-L are higher than those of PLA-S, and those of PLA-S are higher than those of pure PLA. This indicates that GO-L is more beneficial than GO-S to accelerate the crystallization process of PLA and enhance the crystallization ability of PLA.

To intuitively compare the effects of GO-S and GO-L on the nucleation of PLA and the spherulite growth rate of PLA, a temperature of 140 °C, close to the crystallization start temperature of the nonisothermal crystallization curve, was selected. At this temperature, the nucleation ability of PLA itself is weak, which is more conducive to observing the change of nucleation density and crystal growth process after adding GO-S and GO-L. The polarizing microscope images of PLA, PLA-S, and PLA-L treated at 140 °C are shown in Figure 12. It can be seen from the figure that the numbers of spherulites of PLA-S and PLA-L are much more than that of PLA at an isothermal temperature of 10 min, and the numbers of spherulites of PLA-S and PLA-L are not much different, which indicates that GO can play an obvious role in nucleation and the effect of GO size change on the nucleation rate of PLA is small. It can be seen from Figure 13 that the growth rate of spherulites of PLA-L is higher than that of PLA-S, and the growth rate of spherulites of PLA-S is higher than that of pure PLA. Obviously, GO-L has a stronger ability to promote spherulite growth than GO-S.

The 2D-SAXS patterns of pure PLA, PLA-S, and PLA-L after isothermal treatment at 120 °C for 60 min are shown in Figure 14a. From Figure 14a, it can be seen that there is a bright scattering ring in the 2D-SAXS diagram of all samples, indicating that the crystallinities of pure PLA, PLA-S, and PLA-L are large. The corresponding 1D-SAXS pattern (Figure 14b)

https://doi.org/10.1021/acsomega.2c03830
ACS Omega 2022, 7, 37315−37327

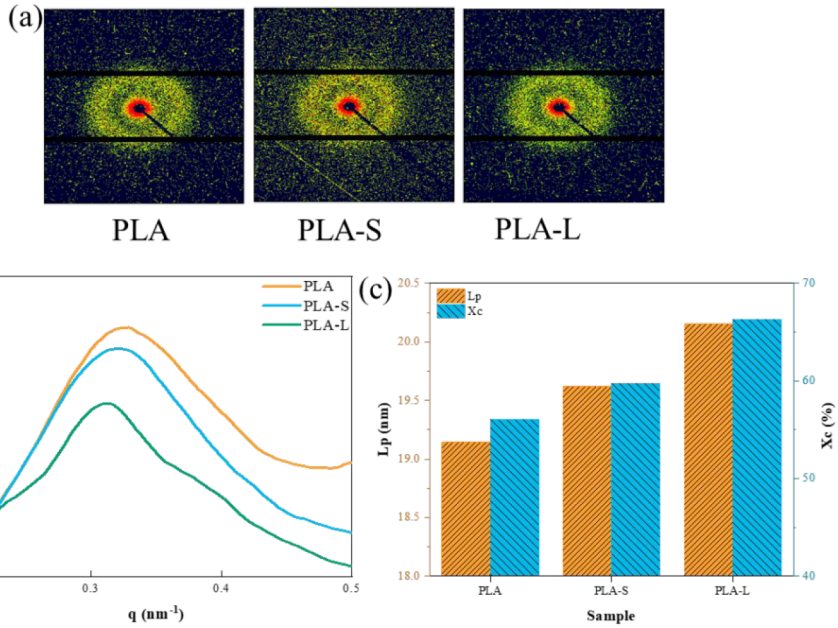

Figure 14. (a) 2D-SAXS patterns, (b) 1D-SAXS curves, and (c) variation of the long period and crystallinity of neat PLA and its nanocomposites after being isothermally crystallized at 120 °C.

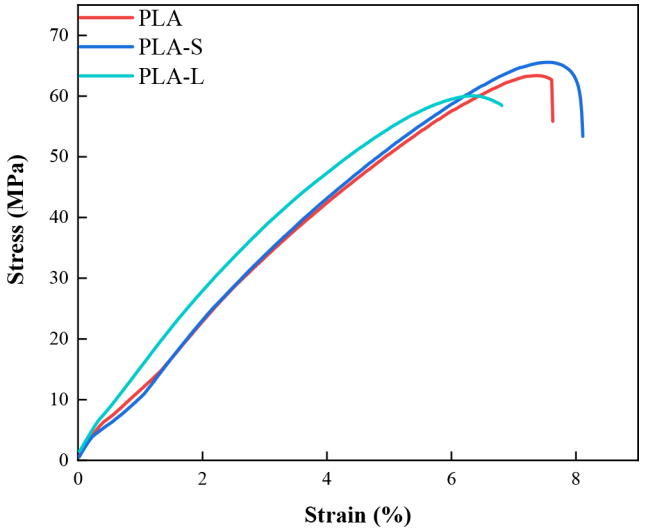

Figure 15. Nominal stress−strain curves of neat PLA and its nanocomposites.

Table 4. Characteristic Parameters of Neat PLA and Its Nanocomposites when Stretching at 25 °C

sample	Young's modulus (MPa)	elongation at break (%)	tensile strength (MPa)	fracture energy (J·m^{-3})
PLA	914.0	7.6	63.4	2.9×10^6
PLA-S	1250.2	8.1	65.6	3.3×10^6
PLA-L	1339.8	6.8	60.0	2.6×10^6

is obtained by integrating the 2D-SAXS pattern in Figure 14a. The relationship between L_p and X_c calculated according to Figure 14b is shown in Figure 14c. It can be seen from Figure 14c that the L_p and X_c of PLA-L are larger than those of PLA-S, and the L_p and X_c of PLA-S are larger than those of pure PLA. The lamellae thickness of PLA-L is larger than that of PLA-S, and the lamellae thickness of PLA-S is larger than that of pure PLA. This is similar to the phenomenon obtained at PLM, and both indicate that GO-L has a stronger ability to promote the growth of PLA crystals.

In general, through the study of crystallization behavior, it can be found that increasing the size of GO can promote the crystal growth of PLA, thereby increasing the crystallinity and accelerating the crystallization process of PLA.

3.4. Mechanical Properties. The stress−strain curves of pure PLA, PLA-S, and PLA-L are shown in Figure 15, and the corresponding result parameters are shown in Table 4. Fracture energy is the energy required for fracture calculated from the area under the stress−strain curve. Compared with elongation at the break, fracture energy can better measure the change of tensile toughness of materials. It can be seen from Table 4 that, after adding GO-S and GO-L, the modulus of PLA is increased from the original 914.0 to 1250.2 and 1339.8 MPa, which are increased by about 40% and 50%, respectively. The fracture energy of pure PLA is 2.9×10^6 J·m^{-3}, that of PLA-S is 3.3×10^6 J·m^{-3}, and that of PLA-L is 2.6×10^6 J·m^{-3}. Compared with pure PLA, the tensile toughness of PLA-S is increased by 12%, and the tensile toughness of PLA-L is decreased by 9%. PLA-S can improve the toughness of PLA while increasing the modulus of PLA, while the increase of the modulus of PLA-L is accompanied by a decrease in toughness. The main reason for this difference is that GO-L has a larger interface surface area, which enables GO-L to transfer stress more effectively and act as a reinforcing filler. However, a larger interface surface area will lead to local internal stress concentration and reduce the toughness of the material.[35]

3.5. Barrier Properties. The gas molecules pass through the polymer mainly through the amorphous region and defects in the crystalline region. The permeation process of gas molecules in polymers is shown in Scheme 2. Gas molecules are first adsorbed on the high-pressure side and then dissolve on the polymer surface. The dissolved gas molecules diffuse to the low-pressure side of the polymer inside the polymer and finally desorb at the low-pressure side. It can be seen from this process that the permeability of gas in the polymer film is

https://doi.org/10.1021/acsomega.2c03830
ACS Omega 2022, 7, 37315−37327

Scheme 2. Permeation Process of Gas in a Polymer Film

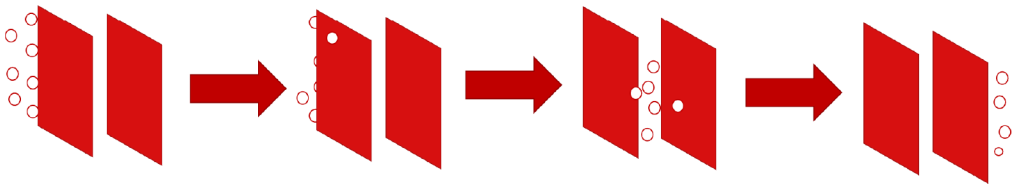

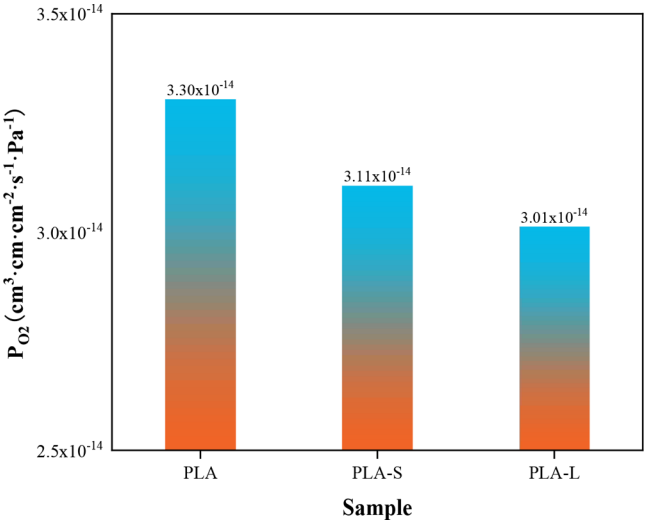

Figure 16. Permeability coefficient of O_2 (P_{O2}) for neat PLA and its nanocomposites films.

mainly affected by two processes of dissolution and diffusion. The gas permeability coefficient P can be calculated by the following formula:

$$P = D \times S \tag{9}$$

where D is the diffusion coefficient of the gas in the polymer matrix and S is the solubility coefficient of the gas on the polymer surface.

The diffusion coefficient (D) of the gas in the polymer matrix can be calculated by the formula

$$D = \frac{L^2}{6t_L} \tag{10}$$

where L is the specimen thickness and t_L is the gas permeation lag time.[36,37]

As can be seen from Figure 16, after adding GO-S and GO-L, P_{O2} of PLA decreased from 3.30×10^{-14} $cm^3 \cdot cm \cdot cm^{-2} \cdot s^{-1} \cdot Pa^{-1}$ to 3.11×10^{-14} $cm^3 \cdot cm \cdot cm^{-2} \cdot s^{-1} \cdot Pa^{-1}$ and 3.01×10^{-14} $cm^3 \cdot cm \cdot cm^{-2} \cdot s^{-1} \cdot Pa^{-1}$, respectively. Under the condition that the filler is well dispersed in the matrix, the gas permeability of the material can be reduced and the gas barrier performance can be improved by adding GO, a nanofiller with a great aspect ratio and impermeability.[15] When GO is distributed on the surface of the polymer matrix, the gas cannot be dissolved at the high-pressure side, reducing the dissolution coefficient of the gas. When GO is dispersed in the matrix, it can make the gas diffusion path longer and more tortuous, so as to increase the gas permeation lag time and reduce the gas diffusion coefficient. These two effects are called the "multipath effect" and "permeable area reduction effect". Because the aspect ratio of GO-L is greater than that of GO-S, P_{O2} of PLA-L is smaller than that of PLA. This shows that GO-L can better improve the barrier properties of PLA.

4. CONCLUSIONS

To ensure the good dispersion of GO-S and GO-L in PLA, pure PLA, PLA-S, and PLA-L were prepared by the solution flocculation method. To ensure that the addition of GO-S and GO-L will not hinder the crystallization of PLA, their addition amount was controlled to 0.1 wt %. In this paper, the effect of the GO size effect on PLA performance is studied. Through the dispersion test, it can be found that both GO-S and GO-L are dispersed in PLA in the form of monolithic layers, indicating that the size variation of GO at lower additions amounts does not affect its dispersibility. It is found by conventional crystallization behavior that GO could significantly improve the crystallinity of PLA. Compared with pure PLA, the crystallinity of PLA-S is increased by about 2.47 times, and the crystallinity of PLA-L is increased by about 2.85 times. It shows that large-size GO is more beneficial to enhance the crystallization performance of PLA. Further research on isothermal kinetics found that the addition of GO can significantly reduce the half-crystal time, and the decrease in the half-crystal time of PLA-L is larger than that of PLA-S, which indicates that large-size GO is more beneficial to accelerate the crystallization process of PLA. The PLM test further reveals that the size variation of GO does not have much of an influence on its nucleation effect on PLA, and the size variation mainly affects the growth process of spherical crystals. From isothermal kinetic studies, it can be shown that the size effect of GO mainly affects the crystallization rate and crystallinity by influencing the spherical crystal growth process. In general, the large size of GO is more favorable to promote the growth of spherical crystals and accelerate the crystallization process, which in turn improves the crystallization properties of PLA. The gas permeability test shows a 5.76% decrease in gas permeability for PLA-S and an 8.79% decrease for PLA-L, indicating that the larger GO size is more favorable for reducing gas permeability and achieving improved barrier performance.

■ ASSOCIATED CONTENT

Supporting Information

The Supporting Information is available free of charge at https://pubs.acs.org/doi/10.1021/acsomega.2c03830.

Comparison table of the enhancement of the barrier properties of PLA by graphene oxide and other fillers (PDF)

■ AUTHOR INFORMATION

Corresponding Authors

Zhihui Xie − *Dongfang Electric Machinery Co., Ltd., Deyang 618000, China*; Email: xiezhihui123@163.com

https://doi.org/10.1021/acsomega.2c03830
ACS Omega 2022, 7, 37315−37327

Jian Kang − *State Key Laboratory of Polymer Materials Engineering, Polymer Research Institute of Sichuan University, Chengdu 610065, China;* orcid.org/0000-0002-3888-2462; Email: jiankang@scu.edu.cn

Authors

Weijiao Jiang − *State Key Laboratory of Polymer Materials Engineering, Polymer Research Institute of Sichuan University, Chengdu 610065, China*

Dandan Chen − *State Key Laboratory of Polymer Materials Engineering, Polymer Research Institute of Sichuan University, Chengdu 610065, China*

Yue Zhang − *Dongfang Electric Machinery Co., Ltd., Deyang 618000, China*

Bo Hu − *Dongfang Electric Machinery Co., Ltd., Deyang 618000, China*

Ya Cao − *State Key Laboratory of Polymer Materials Engineering, Polymer Research Institute of Sichuan University, Chengdu 610065, China*

Ming Xiang − *State Key Laboratory of Polymer Materials Engineering, Polymer Research Institute of Sichuan University, Chengdu 610065, China*

Complete contact information is available at: https://pubs.acs.org/10.1021/acsomega.2c03830

Notes

The authors declare no competing financial interest.

■ ACKNOWLEDGMENTS

We gratefully acknowledge the National Natural Science Foundation of China (NSFC 51503134, 51721091), the State Key Laboratory of Polymer Materials Engineering (Grant No. SKLPME 2017-3-02), and the Fundamental Research Funds for the Central Universities for the financial support. The authors would like to thank Zhang San from Shiyanjia Lab (www.shiyanjia.com) for the XPS analysis and SEM test.

■ REFERENCES

(1) Shi, X. W.; Dai, X.; Cao, Y.; Li, J. W.; Huo, C. G.; Wang, X. L. Degradable Poly(lactic acid)/Metal-Organic Framework Nanocomposites Exhibiting Good Mechanical, Flame Retardant, and Dielectric Properties for the Fabrication of Disposable Electronics. *Ind. Eng. Chem. Res.* **2017**, *56* (14), 3887−3894.

(2) Yang, Y.; Zhang, L. S.; Xiong, Z.; Tang, Z. B.; Zhang, R. Y.; Zhu, J. Research progress in the heat resistance, toughening and filling modification of PLA. *Sci. China-Chem.* **2016**, *59* (11), 1355−1368.

(3) Lim, L.-T.; Auras, R.; Rubino, M. Processing technologies for poly(lactic acid). *Prog. Polym. Sci.* **2008**, *33* (8), 820−852.

(4) Auras, R.; Harte, B.; Selke, S. An Overview of Polylactides as Packaging Materials. *Macromol. Biosci* **2004**, *4* (9), 835−864.

(5) Garlotta, D. A Literature Review of Poly(Lactic Acid). *J. Polym. Environ* **2001**, *9* (2), 63−84.

(6) Södergård, A.; Stolt, M. Properties of lactic acid based polymers and their correlation with composition. *Prog. Polym. Sci.* **2002**, *27* (6), 1123−1163.

(7) Farah, S.; Anderson, D. G.; Langer, R. Physical and mechanical properties of PLA, and their functions in widespread applications - A comprehensive review. *Adv. Drug Delivery Rev.* **2016**, *107*, 367−392.

(8) Standau, T.; Zhao, C. J.; Murillo Castellón, S. M.; Bonten, C.; Altstadt, V. Chemical Modification and Foam Processing of Polylactide (PLA). *Polymers* **2019**, *11* (2), 306.

(9) Pinto, A. M.; Cabral, J.; Tanaka, D. A. P.; Mendes, A. M.; Magalhães, F. D. Effect of incorporation of graphene oxide and graphene nanoplatelets on mechanical and gas permeability properties of poly(lactic acid) films. *POLYM INT* **2013**, *62* (1), 33−40.

(10) Lawal, A. T. Graphene-based nano composites and their applications. A review. *Biosens. Bioelectron* **2019**, *141*, 111384.

(11) de Melo-Diogo, D.; Lima-Sousa, R.; Alves, C. G.; Correia, I. J. Graphene family nanomaterials for application in cancer combination photothermal therapy. *Biomater. Sci.* **2019**, *7* (9), 3534−3551.

(12) Xia, M.-Y.; Xie, Y.; Yu, C.-H.; Chen, G.-Y.; Li, Y.-H.; Zhang, T.; Peng, Q. Graphene-based nanomaterials: the promising active agents for antibiotics-independent antibacterial applications. *J. Controlled Release* **2019**, *307*, 16−31.

(13) Dreyer, D. R.; Park, S.; Bielawski, C. W.; Ruoff, R. S. The chemistry of graphene oxide. *Chem. Soc. Rev.* **2010**, *39* (1), 228−40.

(14) Dikin, D. A.; Stankovich, S.; Zimney, E. J.; Piner, R. D.; Dommett, G. H.; Evmenenko, G.; Nguyen, S. T.; Ruoff, R. S. Preparation and characterization of graphene oxide paper. *Nature* **2007**, *448* (7152), 457−60.

(15) Huang, H. D.; Ren, P. G.; Xu, J. Z.; Xu, L.; Zhong, G. J.; Hsiao, B. S.; Li, Z. M. Improved barrier properties of poly(lactic acid) with randomly dispersed graphene oxide nanosheets. *J. Membr. Sci.* **2014**, *464*, 110−118.

(16) Geng, L. H.; Peng, X. F.; Jing, X.; Li, L. W.; Huang, A.; Xu, B. P.; Chen, B. Y.; Mi, H. Y. Investigation of poly(L-lactic acid)/graphene oxide composites crystallization and nanopore foaming behaviors via supercritical carbon dioxide low temperature foaming. *J. Mater. Res.* **2016**, *31* (3), 348−359.

(17) Zheng, L.; Zhen, W. J. Preparation and characterization of amidated graphene oxide and its effect on the performance of poly(lactic acid). *Iran. Polym. J.* **2018**, *27* (4), 239−252.

(18) Pope, C. G. X-ray diffraction and the Bragg equation. *J. Chem. Educ.* **1997**, *74* (1), 129−131.

(19) Zhang, J.; Sun, X. Mechanical properties and crystallization behavior of poly(lactic acid) blended with dendritic hyperbranched polymer. *POLYM INT* **2004**, *53* (6), 716−722.

(20) Wu, D. F.; Cheng, Y. X.; Feng, S. H.; Yao, Z.; Zhang, M. Crystallization Behavior of Polylactide/Graphene Composites. *Ind. Eng. Chem. Res.* **2013**, *52* (20), 6731−6739.

(21) Avrami, M. Kinetics of phase change I - General theory. *J. Chem. Phys.* **1939**, *7* (12), 1103−1112.

(22) Avrami, M. Kinetics of Phase Change. II Transformation−Time Relations for Random Distribution of Nuclei. *J. Chem. Phys.* **1940**, *8* (2), 212−224.

(23) Park, S. H.; Lee, S. G.; Kim, S. H. Isothermal crystallization behavior and mechanical properties of polylactide/carbon nanotube nanocomposites. *Compos. Part A: Appl. Sci. Manuf.* **2013**, *46*, 11−18.

(24) Lyu, D.; Chen, R.; Lu, Y.; Men, Y. Subsequent but Independent Cavitation Processes in Isotactic Polypropylene during Stretching at Small- and Large-Strain Regimes. *Ind. Eng. Chem. Res.* **2018**, *57* (27), 8927−8937.

(25) Wignall, G. D.; Londono, J. D.; Lin, J. S.; Alamo, R. G.; Galante, M. J.; Mandelkern, L. Morphology of blends of linear and long-chain-branched polyethylenes in the solid state: A study by SANS, SAXS, and DSC. *Macromolecules* **1995**, *28* (9), 3156−3167.

(26) Luo, J. X.; Liu, M. J.; Chen, J.; Min, J.; Fu, Q.; Zhang, J. Effectively maintaining the disentangled state of isotactic polypropylene in the presence of graphene nanoplatelet. *Polymer* **2021**, *226*, 123806.

(27) Yu, Y.-H.; Lin, Y.-Y.; Lin, C.-H.; Chan, C.-C.; Huang, Y.-C. High-performance polystyrene/graphene-based nanocomposites with excellent anti-corrosion properties. *Polym. Chem.* **2014**, *5* (2), 535−550.

(28) Paredes, J. I.; Villar-Rodil, S.; Martinez-Alonso, A.; Tascon, J. M. Graphene oxide dispersions in organic solvents. *Langmuir* **2008**, *24* (19), 10560−10564.

(29) Zhang, T.; Zhu, G.-Y.; Yu, C.-H.; Xie, Y.; Xia, M.-Y.; Lu, B.-Y.; Fei, X.; Peng, Q. The UV absorption of graphene oxide is size-dependent: possible calibration pitfalls. *Microchim. Acta* **2019**, *186* (3), 207.

(30) Wu, D.; Cheng, Y.; Feng, S.; Yao, Z.; Zhang, M. Crystallization Behavior of Polylactide/Graphene Composites. *Ind. Eng. Chem. Res.* **2013**, *52* (20), 6731−6739.
(31) Wang, Y.; Cheng, Y.; Chen, J.; Wu, D.; Qiu, Y.; Yao, X.; Zhou, Y.; Chen, C. Percolation networks and transient rheology of polylactide composites containing graphite nanosheets with various thicknesses. *Polymer* **2015**, *67*, 216−226.
(32) Xu, Z. H.; Niu, Y. H.; Yang, L.; Xie, W. Y.; Li, H.; Gan, Z. H.; Wang, Z. G. Morphology, rheology and crystallization behavior of polylactide composites prepared through addition of five-armed star polylactide grafted multiwalled carbon nanotubes. *Polymer* **2010**, *51* (3), 730−737.
(33) Yasuniwa, M.; Tsubakihara, S.; Sugimoto, Y.; Nakafuku, C. Thermal analysis of the double−melting behavior of poly(L−lactic acid). *J. POLYM SCI POL PHYS* **2004**, *42* (1), 25−32.
(34) Pan, P.; Zhu, B.; Kai, W.; Dong, T.; Inoue, Y. Polymorphic Transition in Disordered Poly(l-lactide) Crystals Induced by Annealing at Elevated Temperatures. *Macromolecules* **2008**, *41* (12), 4296−4304.
(35) Gao, Y.; Picot, O. T.; Bilotti, E.; Peijs, T. Influence of filler size on the properties of poly(lactic acid) (PLA)/graphene nanoplatelet (GNP) nanocomposites. *Eur. Polym. J.* **2017**, *86*, 117−131.
(36) Choudalakis, G.; Gotsis, A. D. Permeability of polymer/clay nanocomposites: A review. *Eur. Polym. J.* **2009**, *45* (4), 967−984.
(37) Compton, O. C.; Kim, S.; Pierre, C.; Torkelson, J. M.; Nguyen, S. T. Crumpled Graphene Nanosheets as Highly Effective Barrier Property Enhancers. *Adv. Mater.* **2010**, *22* (42), 4759−4763.

https://doi.org/10.1021/acsomega.2c03830
ACS Omega 2022, 7, 37315−37327